Characterization of Nanocrystallite CdAl2SO3 Thin Films Produced by Inexpensive Chemical Bath Techniques for Photonic Device Applications: The Influence of Annealing Temperature

J. Ezihe[1]*, D. D. O. Eya[1], C. Iroegbu[1], O. K. Echendu[1,2], K. O. Egbo[1,3]

[1]Department of Physics, Federal University of Technology, PMB 1526, Owerri, Nigeria.

[2]Department of Physics, Qwa Qwa Campus, University of the Free State, X13, Phuthaditjhaba 9866, South Africa.

[3]Department of Physics, City University of Hong Kong, 83 Tat Chee Ave.Kowloon, Hong Kong.

*jamesezihe05@gmail.com

Abstract

Quaternary nanocrystallite ($CdAl_2SO_3$) thin films have been synthesized by the method of chemical bath deposition (CBD) technique using a reaction bath containing cadmium chloride, thiourea, and Aluminium sulphate octadecahydrate at room temperature. The thin films are white in colour and strongly adherent to the substrate. The materials were annealed at various temperatures of 150 °C, 200 °C, and 250 °C before characterizing. The XRD results showed that the $CdAl_2SO_3$ thin films crystallize as binary-phase compounds of $CdSO_3$ and Al_2O_3. The material has good absorbance at room temperature compared to annealed temperature. Annealing has little or no effect on the transmittance of the film material. The absorption coefficient increases with annealing temperature. The reflectance decreases with annealing temperature. The direct bandgap of the $CdAl_2SO_3$ thin films ranges from 3.70eV to 3.9eV. The thickness of the films ranges from 207 nm to 879 nm. The SEM micrographs reveal homogenous and densely packed grains with unequal sizes and shapes. The high absorption in the UV-Vis regions makes the material suitable for thin films absorber solar cells. The direct bandgap of the thin films makes them applicable in optical devices such as LEDs and semiconductor lasers.

Keywords: $CdAl_2SO_3$, thin films, bandgap energy, absorbance.

1.Introduction

Nanocrystallite semiconductor materials have been a huge area of interest for researchers due to their numerous applications in photonics. The nanocrystallite materials differ from the conventional polycrystallite materials by the particle size of which they are composed of, and they show properties that are significantly different from those of conventional material as a result of the large surface to volume ratio, which controls their bulk properties [1]. When particles have dimensions which can be compared to the wavelength of electrons, photons, etc., inside the material, quantum effect plays important role in changing their physical properties especially electrical, magnetic and optical properties. [2]. Nanocrystallite thin films materials can be grown by a dry process or by a wet process depending on the properties of interest of the researcher or manufacturer. Nanocrystallite thin films can be used as a high efficient and low cost semiconductor and photovoltaic devices. [3].

The present work makes use of chemical bath deposition (CBD) technique for the growth of the nanocrystallite $CdAl_2SO_3$ thin film material. CBD is mostly used for the preparation of chalcogenide films. The deposition can be carried out under low temperatures. CBD is a simple and low cost techniques compared to other thin films deposition methods such as: vacuum evaporation, molecular beam epitaxy, sputtering techniques, chemical vapour deposition (CVD), Spray Pyrolysis. It is the simplest as no elaborate arrangement is required. Multi-phased thin film materials can be prepared by this technique. It is possible to grow films over a wide surface area and stoichoimetery. The method is suitable for uniform film coating on substrate of any desired shape and form. [4]. The bath parameters such as ionic concentration, pH, complexetion, and deposition time can easily be controlled for a good and adherent films deposition on the substrate.

The CdAl$_2$SO$_3$ thin films material is a quaternary semiconductor from II-III-VI group, and it is a chalcogenide material. Chalcogenide quaternary thin films had been reported in the literatures. [5-8].

The nanocrystallite CdAl$_2$SO$_3$ thin films had not been reported in the literature to the best of our knowledge. This is the main reason we embarked on the research work to find the properties of the films material for possible photonic applications. The CdAl$_2$SO$_3$ has a very high absorbance in the UV-Vis region of the electromagnetic region which makes it a suitable material for UV-shield and solar absorber material in thin films solar cells.

In the present work, the calculations of the structural and optical properties were done using the literatures [9-20]. The result of the CBD and characterization of the samples after post-deposition annealing are discussed in the sections below.

2. Experimental detail

2.1 Bath constituent and deposition of film

The reaction bath for nanocrystallite CdAl$_2$SO$_3$ thin films consists of 50 ml beaker which contains 5 ml of 0.75 M CdCl$_2$, which was the precursor for cadmium ion. 5 ml of 0.9 M of ethylene-diamine-tetraacetic acid (EDTA) was added to the solution with stirring which was the complexing agent. After which 5 ml of 0.75 M Al$_2$(SO$_4$)$_3$.18H$_2$O was added with stirring which was the precursor for aluminium ion. Thereafter, 5 ml of 1.5 M NH$_3$ was emptied into the beaker with continued stirring, which was the pH stabilizer. Finally, 5 ml of 0.75 M thiourea was added with continued stirring, which was the precursor for sulphur ion. 25 ml of distilled water was added to make the solution up to 50 ml. The entire solution was stirred very well before the insertion of the glass substrate vertically downward into the beaker with the aid of the synthetic form for suspension and also prevention of dust and other particles from entering the solution. Prior to the deposition, the substrates were degreased by dipping them in Concentrated-HCl for 42 hours, washed with detergent, rinsed with distilled water and dried in air. The reaction parameters such as pH, ionic concentration and period of deposition were optimized. The reaction bath was constituted at room temperature.

The bath was left for about 62 hours, after which the slides were removed, rinsed in distilled water and dried in air.

The chemistry for the reactions is given as follows:

The reaction between cadmium chloride (CdCl$_2$), and EDTA formed the metallic complex [Cd(EDTA)]$^{2+}$.

$$CdCl_2 \ + \ EDTA \ \leftrightarrow \ [\ Cd \ (EDTA)]^{2+} + \ 2Cl^- \qquad (1)$$
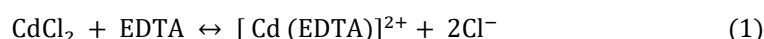
The Cd^{2+} was released into the solution by the metallic complex later.

$$[Cd \ (EDTA)]^{2+} \leftrightarrow \ Cd^{2+} \ + \ EDTA \qquad (2)$$

Aluminium ion Al^{3+} was released from aluminium sulphate octadecahydrate   Al$_2$(SO$_4$)$_3$.18H$_2$O into the solution by the reaction below

$$Al_2(SO_4)_3.18H_2O \ + (\ NH_3) \leftrightarrow 2[Al_2(NH_3)]^{3+} \ + \ 3(SO_4)^{2-} + 18H_2O (3)$$

Then, in ambience

$$2[Al_2(NH_3)]^{3+} + 3O_2 \ \leftrightarrow 2Al^{3+} + \ 6O^{2-} \ + \ NH_3 \qquad (4)$$

The precursor for sulphur ion is (NH$_2$)$_2$CS of which the hydrolysis gives S^{2-},

According to Eqns (5) and (6).

$$(NH_2)_2CS + OH^- \leftrightarrow (NH_2)_2CO + HS^- \tag{5}$$

$$HS^- + OH^- \leftrightarrow S^{2-} + H_2O \tag{6}$$
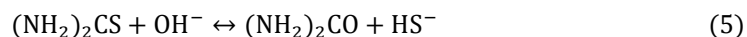
Then the four ions react giving:

$$Cd^{2+} + 2Al^{3+} + 3O^{2-} + S^{2-} \leftrightarrow CdAl_2SO_3(\downarrow) \tag{7}$$

Thus the whole process of deposition gives

$$[Cd\,(EDTA)]^{2+} + 2[Al_2(NH_3)]^{3+} + (NH_2)_2CS + 2OH^- + 3O^{2-} \leftrightarrow CdAl_2SO_3(\downarrow) + EDTA + (NH_2)_2CO + NH_3 + H_2O \tag{8}$$
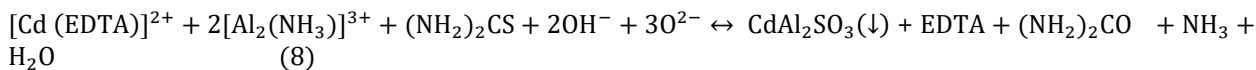
The thin films materials were later annealed at different temperatures of 150 °C, 200 °C and 250 °C, after which they were characterized for their structural, optical, morphological and compositional properties using glancing incident X-ray diffraction (GIXRD), UV-Vis-NIR spectrophotometer, scanning electron microscope (SEM), and energy dispersive x-ray (EDX) respectively. The results of these characterizations are presented and discussed in the next section.

3. Results and discussion

3.1 Structural Analysis

The GIXRD pattern clearly show that the quaternary material cadmium aluminium sulphite (*CdAl₂SO₃*) forms as a multi-phased compound with a combination of *CdSO₃* (monoclinic) and *Al₂O₃* (monoclinic) as indicated by the diffraction peaks corresponding to these materials in both as-deposited and annealed forms in figure 1. The diffraction patterns match those of the Joint Committee on Powder Diffraction and Standard (JCPDS) ref. file number PDF 781474 and PDF 861410, respectively. Multiphase thin-film materials had been reported by many researchers: [21-24].

The as-deposited material has the intensity with the highest peak at about 10000 (arb. unit). At annealing temperature of 150°C, no noticeable change of the intensities of the peaks were observed as the highest peak is still at the region of 10000 (arb. unit) intensity. At 200°C, the highest peak rose to about 15000(arb. unit), and at 250°C the highest peak rose to about 20000 (arb. unit) intensity. These simply show that increase in annealing temperature increases the preferential orientation of the crystallites of the material. The increment of the annealing temperature also gave improved crystallization indicated by narrower peaks shown by the reduction in width for full width at half maximum (FWHM).

The highest peak has the value of 2θ equal to 12.6 degrees with the orientation of (011), which is the preferred orientation of the crystallite (atoms) for both as-deposited and annealed material.

The crystallite size (D) using the major peaks was calculated by Scherrer's equation (9).

$$D = \frac{0.94\lambda}{\beta cos\theta} \tag{9}$$

Where λ is the wavelength of the X-ray and is equal to 1.5406 Å , β is the full width at half maximum of the diffraction peak and θ is the Bragg's angle in degrees.

The interplanar spacing, d, is calculated using the Bragg equation (10).

$$d_{hkl} = \frac{n\lambda}{2sin\theta} \tag{10}$$

Where λthe X-ray wavelength is θ is the diffraction angle and n is an integer.

Table 1 shows the summary of the structural parameters obtainable from the GIXRD analysis for CdAl$_2$SO$_3$, using Eqs (9) - (10).
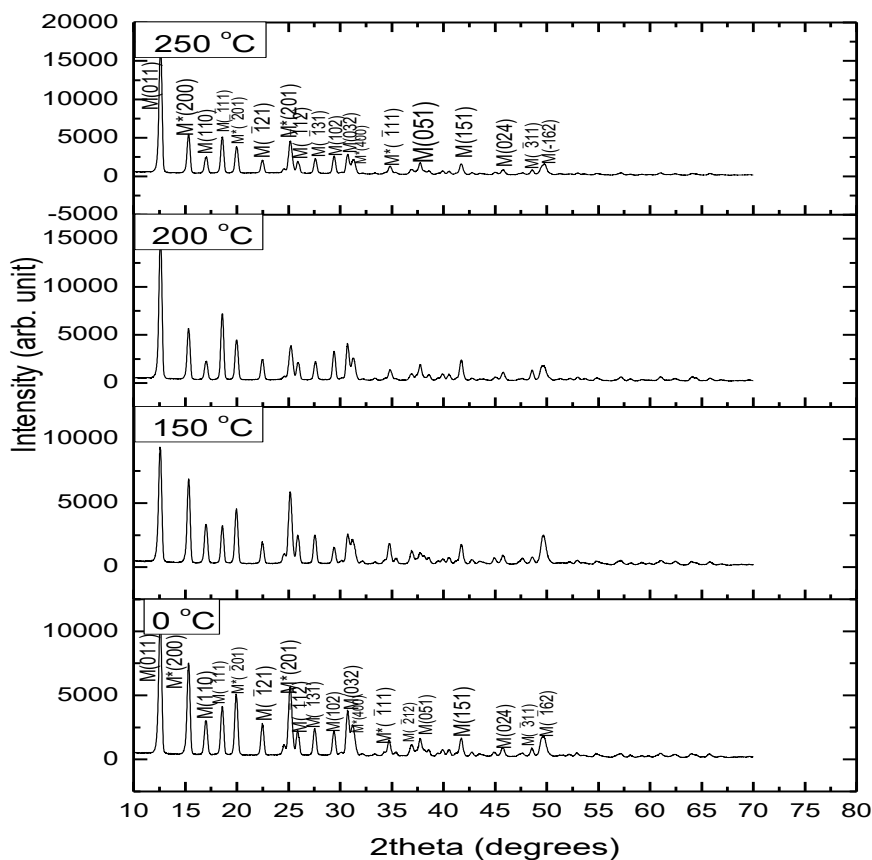
Fig.1 GIXRD patterns of as-deposited and annealed nanocrystallite CdAl$_2$SO$_3$ thin films, showing the presence of a mixture of monoclinic CdSO$_3$ (M) and Al$_2$O$_3$ (M*).

Table 3.1 shows the summary of the structural parameters obtained from the GIXRD patterns for the CdAl$_2$SO$_3$ thin films in both as deposited and annealed form. The table shows mixture of CdSO$_3$ (monoclinic) and Al$_2$O$_3$ (monoclinic) planes of different orientations; with prefer orientation of (011). The table also give the full width at half maximum for as deposited and annealed material having comparable values as well as inter-planar spacing, but the inter-planar spacing decreases as the 2theta values increases for both as deposited and annealed thin films material. However, the crystallite sizes slightly increase after post-deposition annealing of the thin films material.

Table 1 Crystal structure parameters of as-deposited and annealed

CdAl$_2$SO$_3$ thin films.

As-deposited					Annealed					
2θ (°)	(hkl)	β (°)	d-spacing (Å)	D (nm)		2θ (°)	(hkl)	β (°)	d-spacing (Å)	D (nm)
12.6	M(011)	0.3632	7.02	22.99	150°C	12.6	M(011)	0.3544	7.02	23.56

2θ	hkl			
15.3	M*(200)	0.3451	5.79	24.26
17.0	M(110)	0.3676	5.21	22.83
18.6	M($\bar{1}$11)	0.3597	4.77	23.38
19.9	M*($\bar{2}$01)	0.3482	4.46	24.2
22.5	M($\bar{1}$21)	0.3461	3.59	24.45
25.2	M*(201)	0.4089	3.53	20.8
27.5	M($\bar{1}$31)	0.3645	3.24	23.45
30.7	M(032)	0.4093	2.91	21.03

M = CdSO3 Monoclinic

M* = Al2O3 Monoclinic

	2θ	hkl			
	15.3	M*(200)	0.3633	5.79	24.82
	18.6	M($\bar{1}$11)	0.3292	4.77	25.54
	19.9	M*($\bar{2}$01)	0.3317	4.46	25.40
	25.1	M*(201)	0.3975	3.55	21.39
200°C	12.6	M(011)	0.3520	7.02	23.72
	15.3	M*(200)	0.3633	5.79	23.05
	18.6	M($\bar{1}$11)	0.3473	4.77	24.21
	20.0	M*($\bar{2}$01)	0.3537	4.44	23.83
	25.2	M*(201)	0.4581	3.53	18.56
250°C	12.6	M(011)	0.3412	7.02	24.47
	15.3	M*(200)	0.3367	5.79	24.87
	18.6	M($\bar{1}$11)	0.3329	4.77	25.26
	19.9	M*($\bar{2}$01)	0.3350	4.46	25.15
	25.2	M*(201)	0.4023	3.53	21.14

Parameters for the JCPDS reference file 781874, i.e. $CdSO_3$ 2θ = (12.7, 17.7, 19.1, 22.8, 27.8, 30.2) ° and JCPDS reference file 861410, i.e. Al_2O_3 2θ = (15.5, 19.6, 25.1) ° respectively.

3.2 Optical Properties of nanocrystallite CdAl$_2$SO$_3$ Thin films

The optical characterization result for the CdAl$_2$SO$_3$ thin films are presented below.

3.2.1 Transmittance (T)

Fig. 2 shows graph of the transmittance against wavelength for the as-deposited and post-deposition annealed nanocrystallite CdAl$_2$SO$_3$ thin films.

The as-deposited material has a transmittance of about 3.5 % in the NIR-region which increases to about 3.9 % in the Vis-region and falls in the UV-region. The 200 °C annealed sample has about 4.6 % transmittance in the NIR-region which rises to about 5 % in the Vis-region and falls in the UV-region. The 250 °C annealed sample has about 5 % in the NIR-region, which increases to about 6 % in the Vis-region and falls in the UV-region of the solar spectrum. These show that the transmittance of the nanocrystallite material is slightly affected by annealing temperature. That is, increase in annealing temperature increases transmittance.

Generally, the transmittance of the thin films is almost uniform in the NIR-region, which rises slightly towards the Vis-region and falls across the UV-region of the solar spectrum. The reason for poor transmittance being that the material is an opaque material. This poor transmittance shows that the material will not be a good window material for thin films solar cells but suggests that it will be very good for solar absorber material in thin films solar cells.

3.2.2 Absorbance (A)

The graph of optical absorbance versus wavelength for as-deposited and post-deposition annealed $CdAl_2SO_3$ thin films material is shown in figure 3.3, for the wavelength range of 300 nm to 900 nm. From the figure, the highest absorption occurs at the UV-region of the electromagnetic spectrum, with as-deposited sample having absorption of about 99.5% at wavelength of 300 nm, followed by 250 °C annealed sample with absorption of about99.3% , followed by 200 °C annealed film with the absorption of about99%, and fianlly 150°C annealed film with absorption of about98.8%, respectively all at 300 nm wavelength.

We observed that absorption in the UV-spectrum is exact reversal of the absorption in the visible-near infrared spectrum for annealed materials only. The 250 °C annealed sample that is the highest annealed in the UV-spectrum is the lowest in the Vis-NIR spectrum falling to about 94%, followed by 200 °C sample that falls to about 94.5%, and finally 150 °C sample that falls to about 95% in that order.

The as-deposited material maintained the lead in absorption both in the UV-region and Vis-NIR region. This reaffirms that annealing condition used did not increase the absorbance of the thin material. The material gives optimum absorbance in as-deposited form.

Due to the very high absorbance of the $CdAl_2SO_3$, it is suited for absorber material for thin films solar cells. The material can also be used in UV-shielding due to its high absorption in the UV-spectrum.

3.2.3 Reflectance (R)

Fig. 4 shows the reflectance against wavelength for as-deposited and post-deposition annealed CdAl₂SO₃ thin film material. The material generally has very low reflectance for as-deposited and annealed samples across the UV-Vis-NIR regions of the solar spectrum. The reflectance is lower in the UV-region compared to Vis-NIR region. The 250 °C annealed sample has the lowest reflectance in both UV and Vis-NIR region. It has about 0.3% reflectance in the UV which rose to about 1% in the visible and falls to about 0.6% in the NIR-region. The 200°C annealed sample has about 0.7% in the UV, which rose to about 1.3% in the visible, and falls to about 0.8% in the NIR-spectrum. The 150°C annealed sample has 0.9% in the UV which rose to 1.5% in the visible and falls back to 1.0% in the NIR-region.

The as-deposited sample also have the same behaviour as the annealed samples taking low value of reflectance in the UV-region, then rising in the visible region and falling in the NIR-region with the values of 0.4% in the UV, 1.2% in the visible and 0.8% in the NIR-region.

The poor reflectance property makes the material very good for anti-reflection applications.
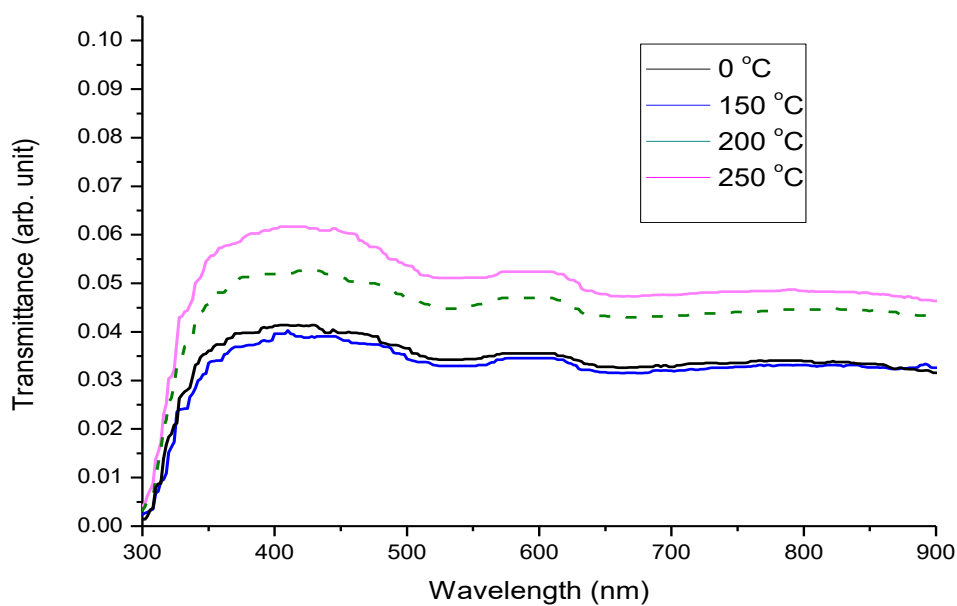
Fig. 2 Optical transmittance against wavelength for as-deposited and post-deposition annealed nanocrystallite CdAl$_2$SO$_3$ thin films
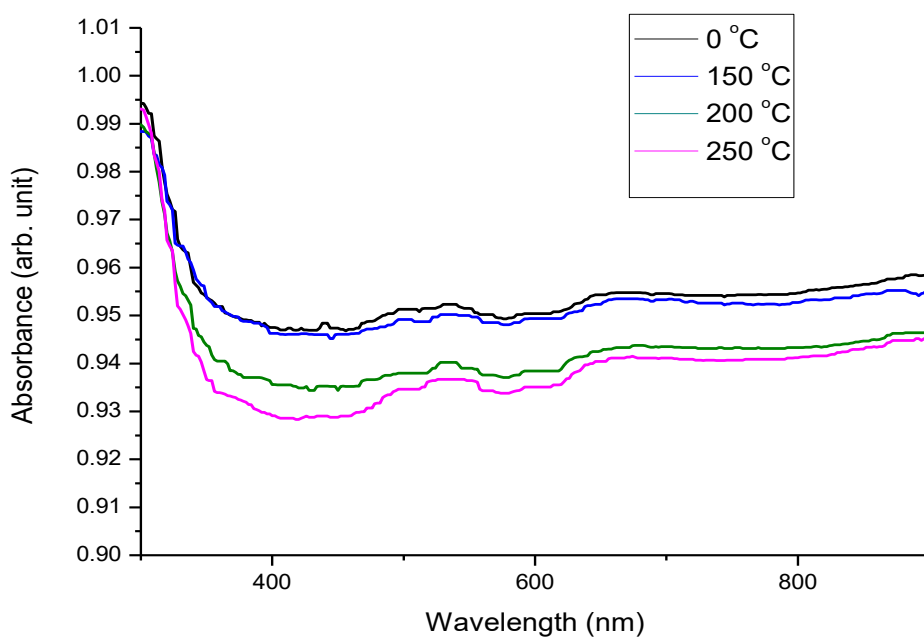
Fig. 3 Optical absorbance against wavelength for as-deposited and post-deposition annealed CdAl$_2$SO$_3$ thin films.
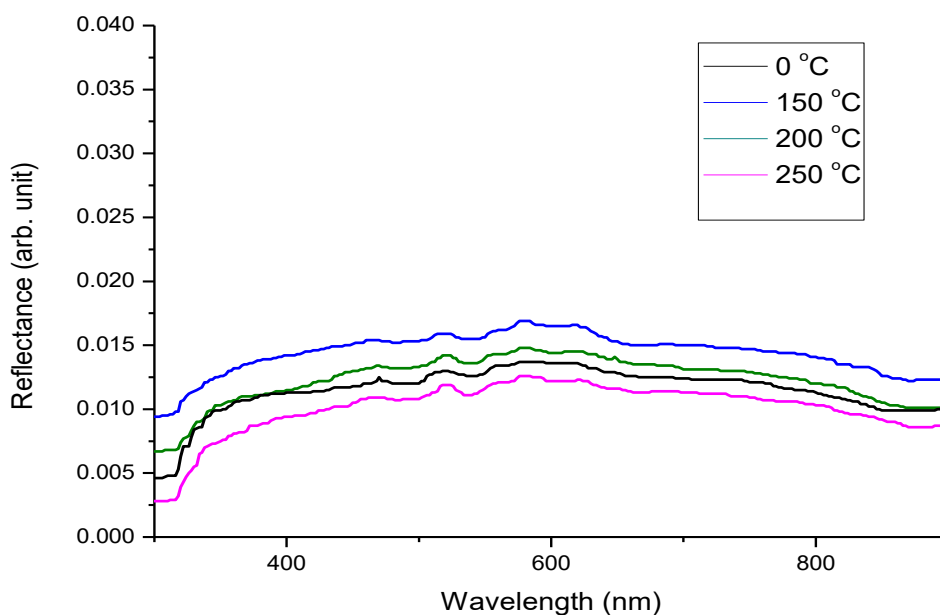
Fig. 4 Optical reflectance versus wavelength for as-deposited and post-deposition annealed $CdAl_2SO_3$ thin films.

3.2.4 Absorption Coefficient (α)

The graph of absorption coefficient against photon energy for both as-deposited and annealed $CdAl_2SO_3$ thin films is shown in fig. 5. It is observed that the absorption coefficient for the annealed materials is higher than that of the as-deposited material. This could be due to densification of the films when annealed. The as-deposited material has absorption coefficient of about 6.0×10^6 m^{-1} close to the absorption edge of photon energy, i.e., 3.68 eV to 3.88 eV. The annealed materials have the absorption coefficient in the range of 12.5×10^6 m^{-1} to 21.0×10^6 m^{-1} near to the absorption edge of the solar spectrum. The absorption coefficient is fairly uniform for both annealed and as-deposited materials in Vis-NIR regions of the electromagnetic region, but rises in the UV-region. The as-deposited material has its highest α of about $6.0 \times 10^6 m^{-1}$ at photon energy of 4.0eV. The annealed materials have their highest absorption coefficient α in the range of 12.5×10^6 m^{-1} to 21.0×10^6 m^{-1}. The trend shows that absorption coefficient increases with annealing temperature. The best annealing temperature for the material with the highest absorption coefficient is 250 °C. Generally, the material has high absorption coefficient which increases as photon energy increases. This again suggests that the material will be a good solar absorber for thin films solar cells.
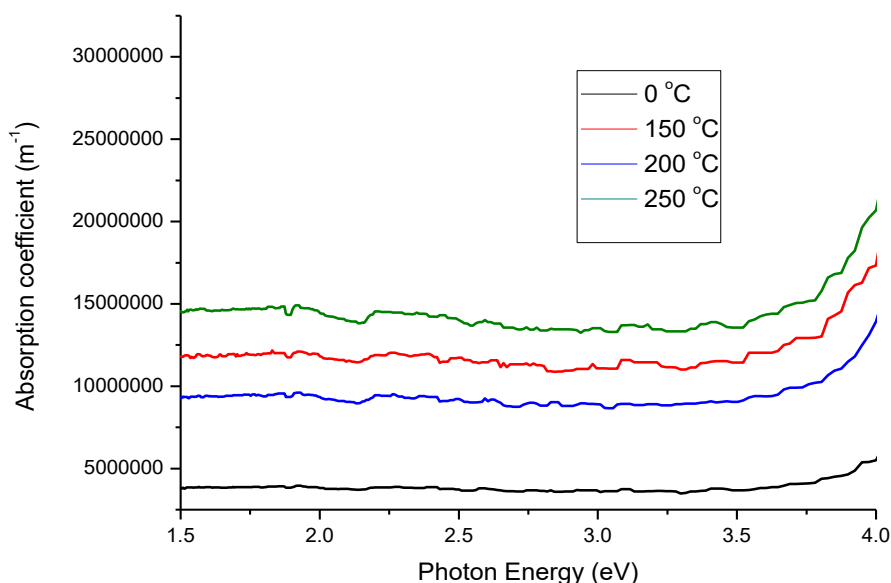
Fig. 5 Absorption coefficient (α) versus Photon energy for as-deposited and annealed $CdAl_2SO_3$ thin films

3.2.5 Extinction Coefficient (k)

Fig. 6 shows the graph of extinction coefficient against photon energy for both as-deposited and post-deposition annealed $CdAl_2SO_3$ thin film materials. The materials have high extinction coefficient across the Vis-NIR regions. The lowest extinction coefficient starts in the UV-region which gradually increases towards the visible region and has its highest value in the NIR-region for both as-deposited and post-deposition annealed samples. This means that the photons are absorbed more in the UV-region.

The as-deposited material has a lower extinction coefficient when compared to the post-deposition annealed samples. The as-deposited sample has its highest extinction coefficient of 2.5 at photon energy of 1.5eV, while the highest extinction coefficient for the post-deposition annealed samples is 0.95 at photon energy of 1.5eV for the 250°C sample.

The value of k for both as-deposited and annealed samples decreases as photon energy increases up to photon energy of 3.8eV, after which it begins to increase. The extinction coefficient generally decreases with photon energy.
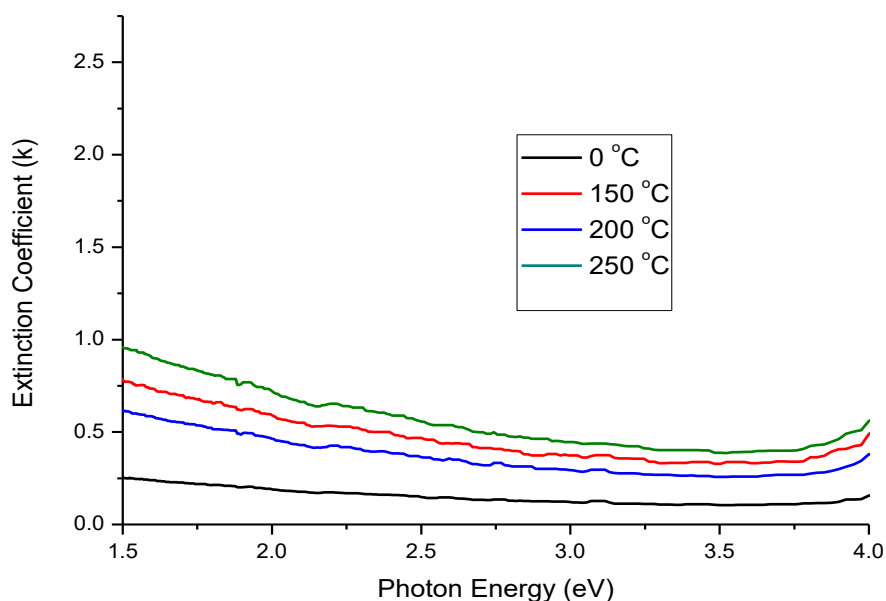
Fig. 6 Extinction coefficient (k) against Photon energy for as-deposited and annealed $CdAl_2SO_3$ thin films

3.2.6 Refractive Index (n)

Fig. 7 shows the graph of refractive index against photon energy for both as-deposited and post-deposition annealed $CdAl_2SO_3$ thin films. In general, refractive index increases as photon energy increases, from NIR-region to visible region. In the visible region it becomes relatively stable, and begins to fall in the UV-region of the electromagnetic spectrum.

The refractive index of as-deposited is 1.15 at photon energy of 0.8eV in the NIR-region and rises to 1.40 in the visible at photon energy of 2.25eV which stood as a major spike, with minor spike on the left at photon energy of 2.0eV and two minor spikes on the right at photon energies of 2.5eV and 2.8eV respectively. The post-deposition annealed samples follow a similar trend. The highest refractive index for annealed samples is 1.43, at photon energy of 2.25eV.

Generally, the refractive index for $CdAl_2SO_3$ thin films material is relatively low, and according to the relation $n = c/v^2$ [16], where v is the propagation speed of light in the medium, and c is speed of light in vacuum. The relation shows that decrease in refractive index will increase the speed of light propagation in the $CdAl_2SO_3$ thin films material. Also, the low refractive index means that there will be very low reflection loss when $CdAl_2SO_3$ material is used for thin films solar cells material.
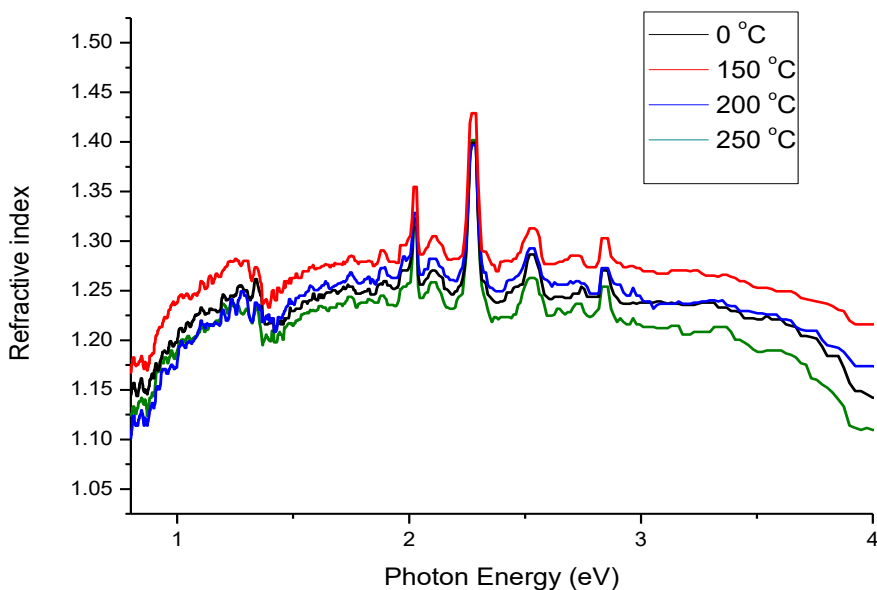
Fig. 7 Refractive index (n) against photon energy for as-deposited and annealed $CdAl_2SO_3$ thin films

3.2.7 Dielectric Constants (ε_r and ε_i)

The spectral response of the real dielectric constant ε_r with photon energy for both as-deposited and post-deposition annealed $CdAl_2SO_3$ thin film materials is shown in fig. 8. The graph shows the same trend as that of the refractive index given in fig. 7.The real part of the dielectric constant ε_r decreases with increasing annealing temperature.

In general, ε_r for as-deposited and post-deposition annealed material is lower in the NIR-region (lower energy region) and gradually rises in the visible region with a huge spike at 2.25eV, which later slightly decreases in the UV-region of the electromagnetic spectrum in relation to photon energy.

The highest value of the real dielectric constant for as-deposited material is 1.9 at photon energy of 2.25eV which stood as a major spike, with minor spike on the left at photon energy of 2.0eV and two minor spikes on the right at photon energy of 2.5eV and 2.8eV respectively. The highest range of values for post-deposition annealed samples is 1.5 to 1.75 at photon energy of 2.25eV. Low dielectric constants favours light propagation in the material medium.

Low dielectric constant in the lower energy region means that devices made with these layers will exhibit relatively low capacitance and thus will display short response time in this photon energy region, recalling that the response time, t, is related to the capacitance, C, and resistance, R, by t =2.2RC.[16],[25]. This material could thus be used in photodetectors.
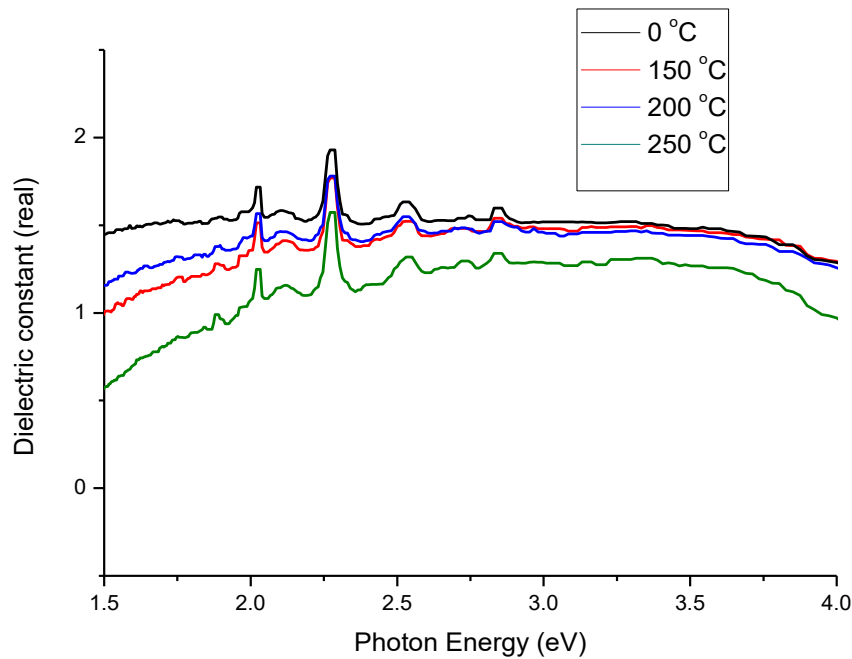
Fig. 8. The spectral response of the real dielectric constant ε_r versus photon energy for as-deposited and post-deposition annealed $CdAl_2SO_3$ thin films

The optical response of the imaginary dielectric constant against photon energy for as-deposited and post-deposition annealed $CdAl_2SO_3$ thin film materials is given in fig. 8. This again shows similar pattern with that of extinction coefficient of fig. 6. The imaginary part of the dielectric constant ε_i increases with an increasing annealing temperature. ε_i generally decreases as photon energy increases.

The highest value of ε_i for as-deposited is 1.6 at photon energy of 1.5eV and the ε_i range for post-deposition annealed samples is 1.5 to 2.28 at photon energy of 1.5eV. The imaginary dielectric constant has its highest values for both as-deposited and annealed samples in the NIR-region which decreases towards the Vis-UV-regions of the electromagnetic spectrum. The observed values of ε_i suggest that devices fabricated at annealing temperature of 250 °C will display relatively improved and more stable capacitance and therefore will have

longer response time in the infrared photon energy range compared to other annealing temperatures.
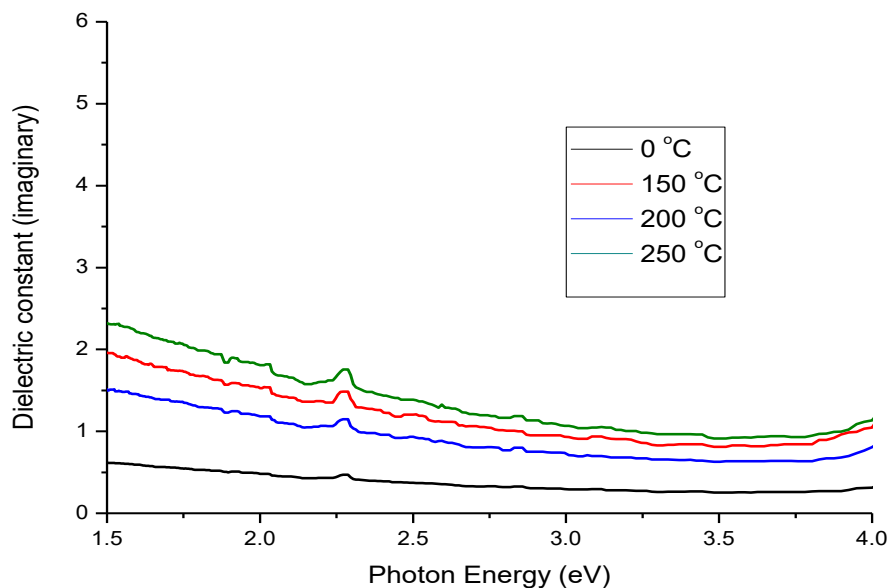
Fig. 9 The spectral response of the imaginary dielectric constant ε_i versus photon energy for as-deposited and post-deposition annealed CdAl$_2$SO$_3$ thin films

3.2.8 Bandgap Energy (E$_g$)

The direct bandgap energy versus photon energy for as-deposited and post-deposition annealed CdAl$_2$SO$_3$ thin films is shown in fig. 10. The graph shows $(\alpha h\nu)^2$ against $h\nu$ which is the famous Tauc method of determining energy bandgap. From the plot, the direct energy bandgap is estimated by extrapolating the straightline portion of the curve (after the absorption edge) to the point where $(\alpha h\nu)^2 = 0$.

The direct bandgap energy, E$_g$ for as-deposited sample was estimated to be 3.90 eV, and the annealed materials have the bandgap in the range of 3.70eV to 3.85eV which is smaller compared to as deposited material. E$_g$ decreases to 3.76 eV at annealing temperature of 150 °C, and then increases to 3.85eV at annealing temperature of 200 °C, and again decreases to 3.70 eV at annealing temperature of 250 °C. Generally, bandgap energy decreases as annealing temperature increases. This could be caused by grain growth [19]. For bandgap energy, the optimal annealing temperature is 250 °C. The wide bandgap energy of CdAl$_2$SO$_3$ thin films can be aligned with materials with narrow bandgap such as SnS thin films reported by researchers to have E$_g$ of the range 1.1eV to 1.5eV to achieve graded bandgap of high quality thin films material for solar energy conversion. The direct bandgap thin films could also be used to make optical devices such as LEDs and semiconductor lasers.
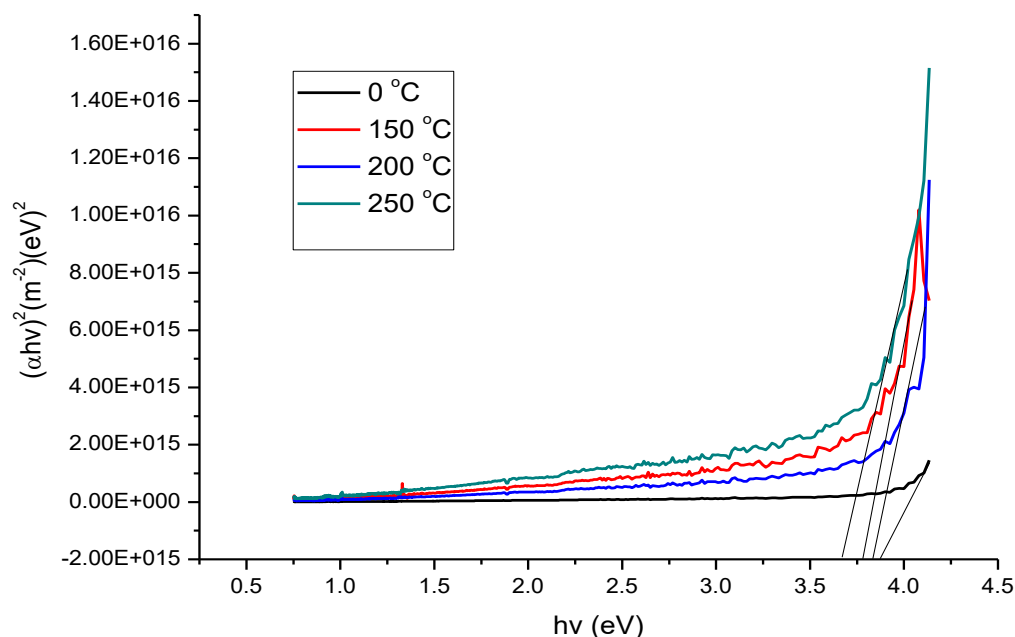
Fig. 10.The energy bandgap versus photon energy for as-deposited and post-deposition annealed CdAl$_2$SO$_3$ thin films

3.3 Film thickness and Compositional Analysis

3D optical profilometery method was used to determine the films thickness of the materials. It is observed that the films thickness generally decreases with increasing annealing temperature.

The as-deposited sample has films thickness of 879 nm and the annealed samples have films thicknesses of 288 nm, 332 nm and 207 nm for annealing temperatures of 150°C, 200°C and 250°C respectively.

The graph of thickness against annealing temperature is given in fig. 11. From the graph, it is observed that at about 27°C i.e. room temperature, the thin films material has the highest value of thickness given as 879nm. Above the room temperature, at annealing temperature of 150°C, there is sharp decrease in thickness. As the annealing temperature increases the thickness decreases. At annealing temperature of 150 °C there is sharp decrease in thickness with the value of 288 nm. At annealing temperature of 200 °C, the thickness increases to 332 nm. And then, at the annealing temperature of 250 °C the thickness falls to 207 nm. The material dependence on annealing temperature is not uniform. The optimal annealing temperature for thickness is 200 °C. For the samples, the as-deposited material gives a better option for photonic applications.

The atomic composition analysis was carried out using energy dispersive X-ray (EDX) spectroscopy. Fig. 12 shows the energy dispersive X-ray spectra of the CdAl$_2$SO$_3$ in both as-deposited and annealed forms. The spectra show the presence of Cd, Al, S and O. Other peaks showing C, N and part of O come from the underlying glass substrate on which these films are grown.
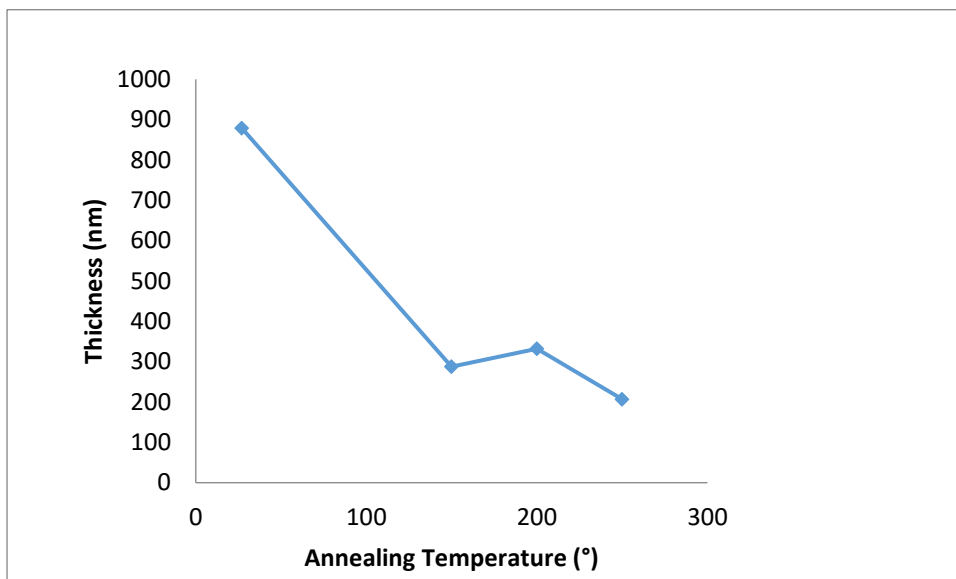
Fig. 11. The graph of thickness against annealing temperature

Close observation of the spectra shows a slight decrease in sizes of the peaks, after post-deposition annealing of the material. This also reaffirms the fact that post deposition annealing reduces the thickness of the films as stated above.

Table 2 shows the percentage atomic concentrations of Cd, Al, S and O in the materials gotten from the analysis of EDX. Fig. 12 and Table 2 show that as-deposited and annealed materials are Al and O-rich. The CdS/O ratio for as-deposited sample is slightly higher than that of the annealed samples. The same trend is repeated for Al/O ratio for both as-deposited and annealed samples.
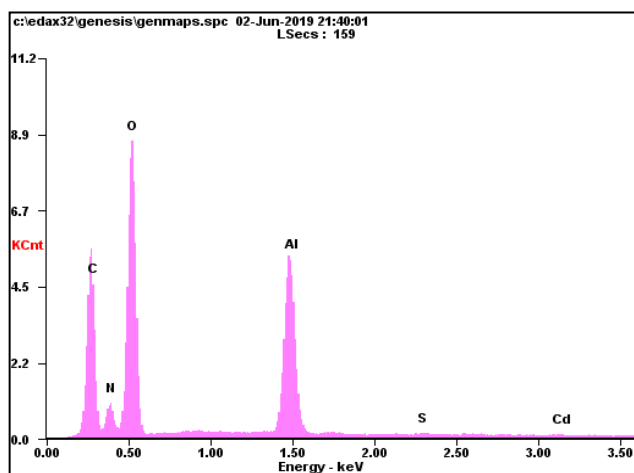
As-deposited   150°C Annealed
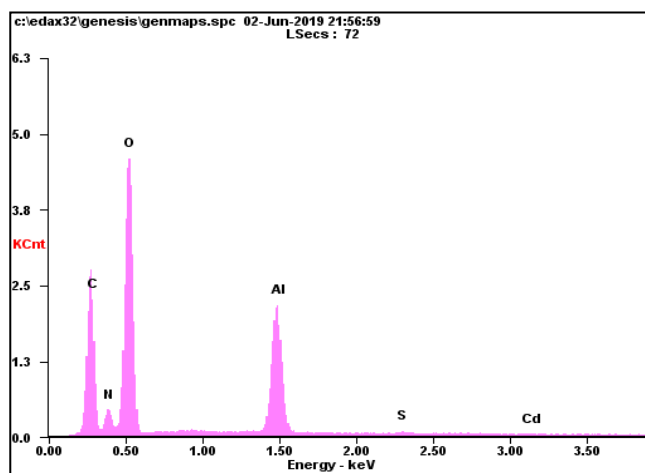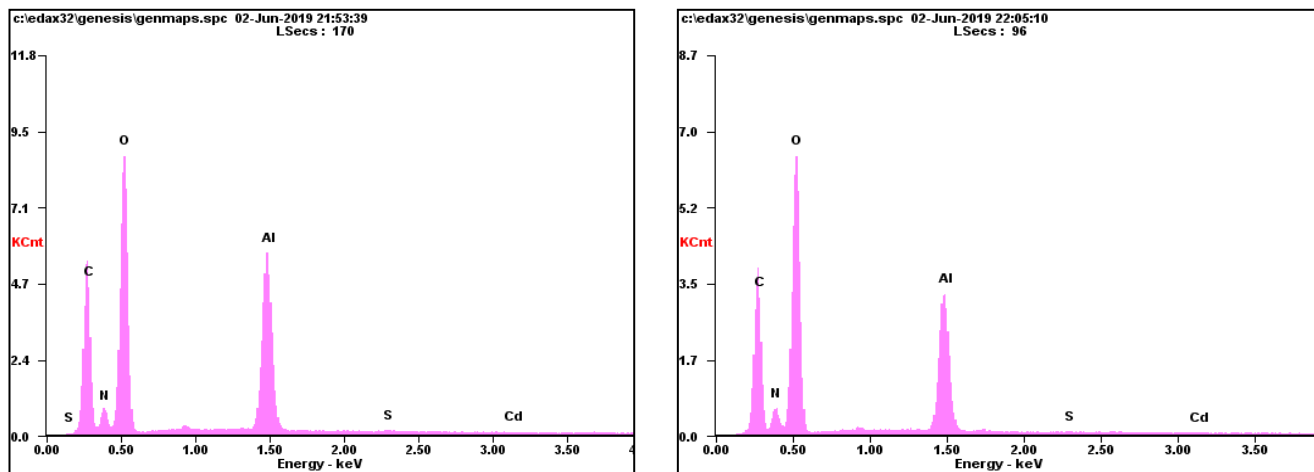
230°C Annealed   250° Annealed

Fig. 12 EDX spectra of as-deposited and annealed $CdAl_2SO_3$ thin films grown by CBD method

Table 2 Percentage atomic compositions of as-deposited and annealed $CdAl_2SO_3$ thin films

As-deposited							Annealed					
Atomic %							Atomic %					
Cd	Al	S	O	CdS/O	Al/O		Cd	Al	S	O	CdS/O	Al/O
0.1	16.08	0.15	83.7	0.0002	0.19	150°C	0.08	13	0.18	86.74	0.00017	0.15
						230°C	0.04	16.97	0.12	82.87	0.000058	0.20
						250°C	0.06	14.27	0.1	85.57	0.000071	0.17

3.4 Morphological Analysis

The scanning electron microscopy is a convenient method for studying the surface morphology of a material. Fig. 13 shows SEM micrographs of the as-deposited and annealed $CdAl_2SO_3$ thin films samples. These images show that the post-deposition annealing has no noticeable effect on the morphology of the $CdAl_2SO_3$ samples. It is observed that the grains are homogenous and densely packed. It is also noticed that the grains are small with unequal sizes and shapes with sharp edges showing crystallinity. Isolated clusters were also observed from the SEM images of the materials especially for annealed samples.

Due to the dense nature of the grains, it was difficult to measure grain sizes. However, close observation and careful estimation gave the grain sizes of the range (20-70) μm for the as-deposited sample and (15-50) μm for annealed samples. These values show that the material sizes decrease with increasing annealing temperature.
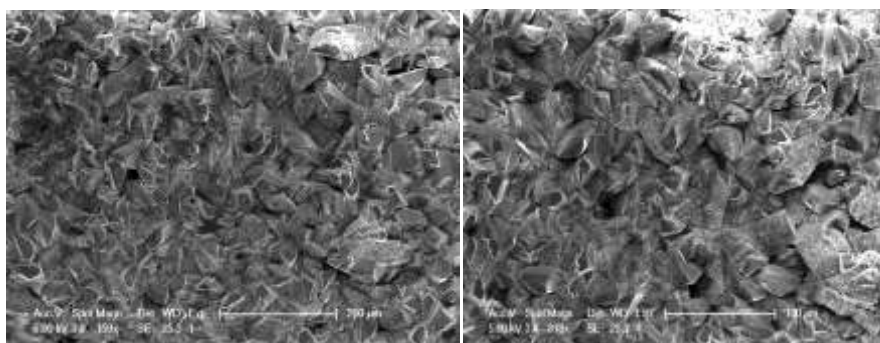
A1 As-deposited   ×159   **A2 As-deposited ×318**
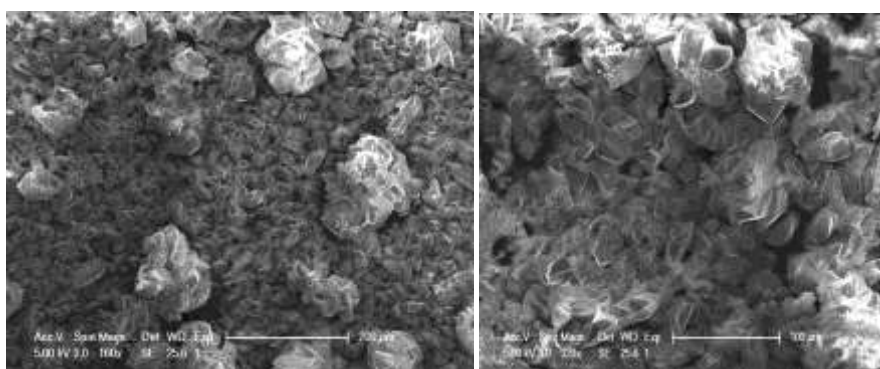
B1-150°C Annealed ×160   B2-150°C Annealed ×320
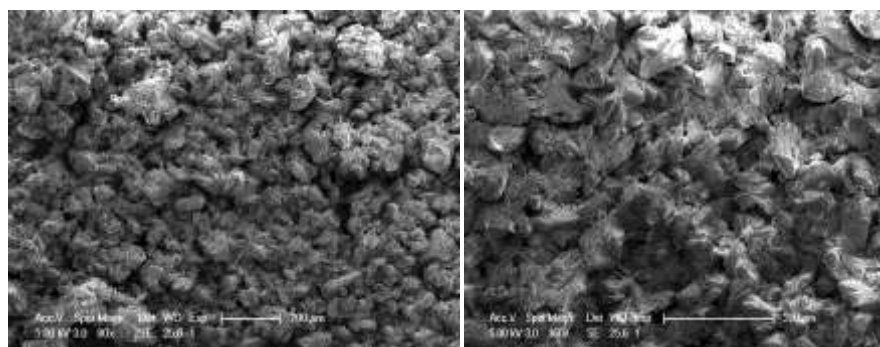
C1-200°C Annealed ×80   C2-200°C Annealed ×160
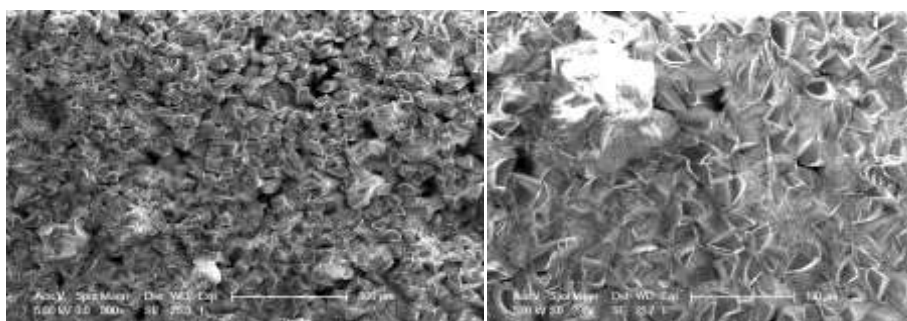
D1-250°C Annealed ×300   D2-250°C Annealed ×296

Fig. 13 SEM images of as-deposited and annealed CdAl$_2$SO$_3$ thin films.

4. Conclusion

The nanocrystallite $CdAl_2SO_3$ thin films have been successfully prepared by a cost effective chemical bath deposition (CBD) techniques. The material structural properties, optical and solid state properties, compositional properties and morphological properties were investigated for as-deposited and post-deposition annealed samples. The optical parameters investigated include: transmittance, absorbance and reflectance, absorption coefficient, extinction coefficient, refractive index, dielectric constant and energy bandgap.

The influence of the annealing temperature on the optoelectronic properties of the layers depends on the particular choice of application. The material has good absorbance at room temperature compared to annealing temperature absorbance. Annealing has little or no effect on the transmittance of the film material. The absorption coefficient increases with annealing temperature. The reflectance decreases with annealing temperature. The high absorption in the UV-Vis regions makes the thin films suitable for use as absorber layer in thin films solar cells. The poor reflectance of the films also indicates that it could be used as anti-reflection material. The direct bandgap of the thin film material makes it applicable in optical devices such as LEDs and semiconductor lasers. These and other unexplored applications can be achieved from the $CdAl_2SO_3$ thin films.

Acknowledgements

Reference

1.   U. Ubale, S. G. Ibrahim, Structural, electrical and optical properties of nanostructural $FeCdS_3$ thin films deposited by chemical spray technique: effect of complex. International Journal of Material and Chemistry, 2(2) (2012): 57-64. DOI: 10.5923/j.ijmc.20120202.03

2.   Aviram, M. A. Ratner, Molecular rectifier, Chem. Physics. Lett. Vol.29 (1974) pp. 277-283.

3.   U. Ubale, K. S. Chipade, M. V. Bhute, P. P. Raut, G. P. Malpe, Y. S. Sakhare, M. R. Belkhedkar, Structural, optical and electrical properties of nanostructured CdS:CuS composite thin films grown by CBD method, International Journal of Materials and Chemistry. 2(4) (2012): 165-172. DOI: 10.5923/j.ijmc.20120204.09

4.   L. O. Onyegbule, Chemical bath deposition and characterisation of SnS and SnS-Cu_xS MSc. Thesis, Federal University of Technology Owerri. (2015)

5.   H. Heujun, H. Guan, L. Lei, Sythesis of Cu_2FeSnS_4 thin films with Stannite and Wurtzite structure directly on glass substrate via the solvothermal method, Journal of Materials Science Materials Electronics. 28(11) (2007). doi: 10.1007/s 10854-017-6469-6

6.   M. Xie, Z. Daming, Z. Ming, Z.Zhuang, O. Liangqi, L. Xiaolong, S. Song,. Preparation and characterization of Cu_2ZnSnS_4 thin films and solar cells fabrication from quaternary Cu-Zn-Sn-S target. International Journal of Photoenergy, Article ID 929454, (2013) 9 pages. http://dx.doi.org/10.1155/2013/929454

7.   M. Lei, L.Yongfeng, Y. Bin, D. Zhan-Hui, Y. Gang, L. Rui-Jian, D. Rui, L. Lei, Mechanism of effect of intrinsic defects on electrical and optical properties of Cu_2CdSnS_4: an experimental and first-principles study, Journal of Physics, Volume 48, (2015) Number 44

8.   M. Xiaohui, C. Ruizhi, C. Wenjuan, Synthasis and characterization of Cu_2FeSnS_4 thin films prepared by electrochemical deposition, Materials Letters, (2017)193. doi. 10.1016/j.matlet.2017.01.099

9.   Majumdar, H. Z. Xu, F. Zhao, L. Jayasingha, S. Khosravani, X. Lu, V. Kelkar, Z. Shi, Mat. Res. Soc. Symp. Proc. 770 (2003)

10.   Dhere. Ramesh, Tim. Gessert, Jie. Zhou, Sally. Asher, Joel. Pankow and Helio. Moutinho, Mat. Res. Soc. Symp. Proc. 763 (2003) 1

11.   K. Shwarsctein, T. F. Jaramillo, Sung-Hyeon. Baeck, M. Sushdhikh and E. W. McFarland, J. Electrochem. Soc. 153(7) (2006) 483

12.   F. C. Eze and C. E. Okeke, Materials Chemistry and Physics, 47 (1997) 31

13.   M. Theye, Thin film technology and applications in optical properties of thin films. K.L Chopra and L. K. Malhota (eds). (Tata McGraw-Hill, New Delhi, 1985) p. 163

14.   R. Rodrigo del, D. Basaure, R. Schrebler, H. Gomez and R. Cordova, Phys. Chem. B106(49) (2002) 12634

15.   Yano. Mitsuaki, Ken-Ichi Ogata, Fengping. Yan, Kazuto. Koike, Shigehiko. Sasa and Masataka. Inoue, Mat. Res. Soc. Symp. Proc. 744 (2003) 1 [16] E. Pentia, V. Draghici, G. Sarau, B. Mereu, L. Pintillie, F. Sava and M. Popeseu, J. Electrochem. Soc. 151(1) (2004) 729

16.   O. K. Echendu, Thin film solar cells all-electrodeposited ZnS, CdS and CdTe materials, PhD. Thesis, Sheffield Hallam University, United Kingdom (2014).

17.   O. K. Echendu, A. R. Weerasinghe, D. G. Disco, F. Fausi, I. M. Dharmadas, Characterisation of n-type and p-type ZnS thin layers grown by electrochemical method, J. Elect. Mater: 42(11) (2013) 692-700.

18.   O. K. Echendu, S. Z.Werta, F. B. Dejene, Effect of Cadmium precursor on the Physico-chemical properties of electrochemically grown CdS thin films for optoelectroniccs devices application: a comparative study, Journal of Material Science: Materials in Electronics. (2019) 30: 365-377.

19.   D. D. O. Eya, F.C. Eze, O. K. Echendu, U. S. Mbamara, Synthesis and optical properties of chemically deposited cadmium sulphide thin films, Nigerial Journal of Solar Energy, Vol. 27(2016).

20.   Mahrov, G. Boschloo, A. Hyfeldt, H. Siegbahn, H. Rensmo, Photoelectron spectroscopy studies of Ru(dcbpyH2)2(NCS)2/CuI and Ru(dcbpyH2)2/CuSCN interfaces for solar cell applications, Journal of Physical Chemistry B. 108 (31) (2004) 11604-11610.

21.   J. R. Bakke, J. T. Tangkanen, C. Hagglund, T. A. Pakkanen, S. F. Ben, Growth characteristics, material properties and optical properties of zinc oxysulphide films deposited by atomic layer deposition, J. Vac. Sci. Technol. A: Vac Surf Films. 30(2012) 01A135-1 - 01A135-8. doi.org/10.1116/1.3664758

22.   Q. Cheng, D. Wang, H. Zhon, Electrodeposition of Zn(OS) (Zinc oxysulfide) thin films: exploiting its thermodynamic and kinetic processes with incorporation of tartaric acid, J . Energy Chem. (2017) https://doi.org/10.1016/j.jechem.2017.07.020(in press)

23.   R. Henriquez, M. Froment, G. Riveros, E. A. Dalchiele, H. Gomez, P. Grez, D. Lincot, Electrodeposition of polyphasic films of zinc oxysulfide from   DMSO onto n-Inp(100) and n-Inp(111) single crystals in the presence of zinc salt, thiourea and dissolved molecular oxygen, J . Phys. Chem. C111(2007) (6017-6023)

24.   Polat, S. Aksu, M. A. Itunbas, , S. Yilmaz, , E. Bacaksiz, The influence of diffusion temperature on the structural, optical and magnetic properties of manganese-doped zinc oxysulfide thin films, J. Solid State Chem. 184(2011) (2683-2689)

25.   R. S. Quimby, Photonics and lasers: An Introduction (Hoboken, NJ: Wiley). P.259, 2006.